

# CALCULATIONS FOR TERA-HERTZ (THZ) RADIATION SOURCES \*

Yasser A. Hussein and James E. Spencer  
SLAC, Stanford University, Menlo Park, CA 94025, U.S.A

## Abstract

We explore possibilities for THz sources from 0.3 - 30 THz. While still inaccessible, this broad gap is even wider for advanced acceleration schemes extending from X or, at most, W band RF at the low end up to CO<sub>2</sub> lasers. While physical implementations of these approaches are quite different, both are proving difficult to develop so yet lower frequency, superconducting RF is preferred. Similarly, the validity of modelling techniques varies greatly over this range but generally mandates coupling Maxwell's equations to the appropriate device transport physics for which there are many options. Here we study radiation from undulatory-shaped transmission lines using finite-difference, time-domain (FDTD) simulations. Also, we present Monte-Carlo techniques for pulse generation. Examples of THz sources demonstrating constructive interference are shown with the goal of optimizing on-chip radiators.

## INTRODUCTION

Recently, we explored possibilities for producing narrow-band THz radiation using either free or bound electrons (solid state) in micro-undulatory periodic configurations [1] because integrated circuit technology appeared well matched to this region extending 2 decades from 1000-10 μm. This range has largely been neglected until recently because it runs from the limit of WR-3 waveguide around 300 GHz up to CO<sub>2</sub> lasers where the laser regime becomes dominant. An excellent review of terahertz technology and its applications in biology and medicine can be found in the papers by Siegel [2]-[3].

There are mainly two approaches for generating THz radiation, i.e. free or bound electron (BE) possibilities. Our emphasis is on the later using IC technology as opposed to FELs that are bulky, expensive, need high power and have low efficiency [4]. While accurate modelling of the proposed implementation requires coupling of Maxwell's equations with an appropriate physics-based transport model, here we concentrate on electromagnetic analysis on the assumption of ballistic transport and that radiative losses dominate other loss mechanisms, i.e. conductor, thermal, and substrate loss.

## DISCUSSION AND ANALOGY

The most direct approach to obtain the radiation pattern is with the Poynting vector from calculating the far-field acceleration pattern and from it the angular distribution:

$$\frac{dP}{d\Omega} = \frac{1}{4\pi c^3} \left\{ \mathbf{n} \times \int \frac{\partial \mathbf{J}(\mathbf{r}', t_r)}{\partial t} d\mathbf{r}' \right\}^2 \quad (1)$$

\*Work supported by U.S. DOE under contract DE-ACO3-76SF00515.

$t_r$  is the retarded time between source and detector,  $\mathbf{J}$  the current density,  $P$  the power, and  $c$  the speed of light. For  $\beta \equiv v/c \ll 1$ , Eq.1 reduces to the Larmor equations:

$$\frac{dP}{d\Omega} = \frac{c^2}{4\pi c^3} \frac{dv(t)^2}{dt} \sin^2 \theta \quad \text{and} \quad P = \frac{2}{3} \frac{e^2}{c^3} \frac{dv(t)^2}{dt} \quad (2)$$

$\theta$  is the angle between the observation direction  $\mathbf{n}$  and the direction of acceleration at emission time  $t$ . A well known application of Eq. (1) was given in Ref. [1] where we noted that a beam of free electrons in an undulator that provides a sinusoidal field with wavelength  $\lambda_u$  would produce harmonics  $q$  of the device wavelength:

$$\lambda = \frac{\lambda_u}{2q\gamma^2} \quad (3)$$

where the electron energy  $\gamma$  is in units of  $mc^2$ . To increase photon frequency, one increases  $\gamma$  or reduces  $\lambda_u$  or the effective mass  $m^*$ . For conduction-band electrons,  $\gamma \sim 1$  so that a wiggle period of  $\lambda_u = 60 \mu\text{m}$ , achievable with standard IC techniques, might be expected to give  $30 \mu\text{m}$ , 10 THz radiation with angular spread  $\sim 1/\gamma$  or one radian.

## NOMENCLATURE

In a typical, 2-port, passive, microwave structure, the power dissipated (normalized to the input power) can be estimated on the assumption that the S-matrix is complex and orthogonal as:

$$P_i = 1 - |S_{11}|^2 - |S_{21}|^2 \geq 0 \quad (4)$$

The power dissipated can be due to radiation, conductor or substrate loss. For instance, for a standard radiating structure with no output port ( $S_{21}=0$ ), the dissipated power is dependent on  $S_{11}$  only so that small values of  $S_{11}$  indicate high loss. Further, we assume that the conductor and substrate loss are much less than radiation loss. The radiated power in this case goes inversely as  $|S_{11}|^2$ . One can then define the radiation efficiency which is verified by the calculations here as:

$$\eta = \frac{P_r}{P_i} \quad (5)$$

where  $P_i$  is the total applied power - ideally the so-called wall-plug power that we typically take as 1W.

Finite-Difference, Time-Domain (FDTD) is a powerful and flexible technique that is expected to play a central role in development and simulation of sub-millimeter wave devices [5]. It is ideal for our problem where future research may include anisotropies and nonlinearities, and where high pulsed currents are important. Figure 1 gives sample comparison curves between the FDTD codes developed here and HFSS for the radiation efficiency. These results were obtained by simulating the structure shown in Fig. 2 with the indicated dimensions.

In Fig. 1, the radiation efficiency is estimated from the FDTD calculations using Eqs. 4-5. HFSS obtains this by integrating the far-field, Poynting vector. Finally, we note that Fig. 1 also validates Eq. (4).

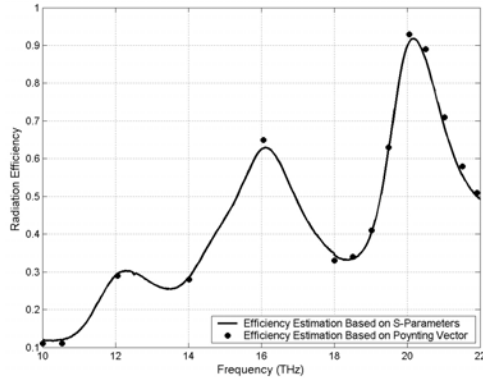


Figure 1: Radiation efficiency for structure in Fig. 2 for  $d=2.0$ ,  $R=3.6\mu\text{m}$ . Solid line is FDTD, dotted is with HFSS.

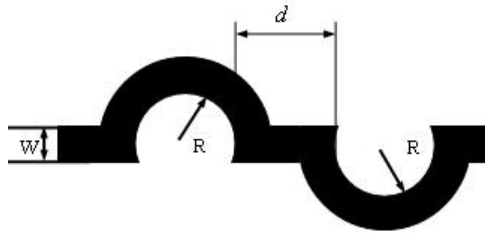


Figure 2: Metallic top-view of opposing half-circles separated by distance  $d$ ,  $R=4$ ,  $W=2\mu\text{m}$  and  $d \geq W$ . Tuning parameters are impedance  $w/h$ , shape  $R$ , phase  $d$  and  $\epsilon$ .

### RADIATION CALCULATIONS

Detailed HFSS simulations were done for the radiation patterns of several configurations. The half-period layout and radiation pattern for  $\varphi=90^\circ$  (the YZ plane) is in Fig. 3. Higher frequencies have higher radiated power while  $S_{11}$  trends higher and  $S_{21}$  decreases. At higher frequencies, the  $90^\circ$  turns put in to avoid i/o crosstalk and define loops, begin to be resolved

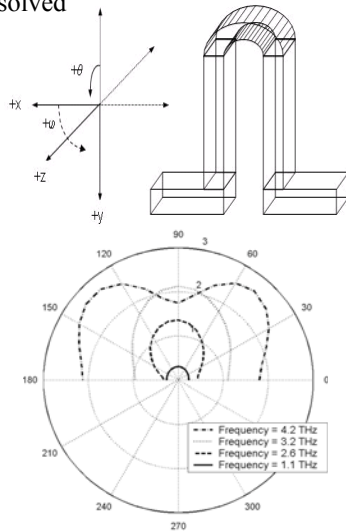


Figure 3: Radiation pattern for total E-field at  $\varphi = 90^\circ$  with radial scale in V/m for a normalized input of 1 W.

We view these as two dipoles at  $90^\circ$  to one another, which become dominant at the highest frequency where they produce the double-lobed distribution. From Eq's.2, these show angular spreads of  $\sim 1/\gamma$  and, as long as  $\lambda \gg l$ , with  $l$  a characteristic size, the power should peak at  $90^\circ$  and vary as frequency squared. This appears true for Fig's.4-5.

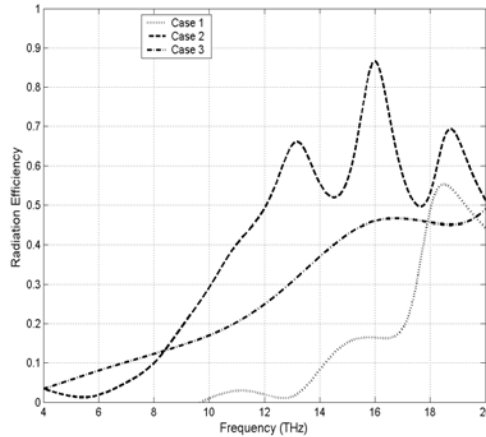


Figure 4: Here  $d=W$  in Fig. 2. Case 1: single half-circle. Case 2: two half-circles. Case 3: two half-circles without  $90^\circ$  turns done by rearranging ports.

#### Case 1: 2-Loop, 1-Period, $N=1$ , $d=W$ Examples

Three cases corresponding to modifications of Fig. 2 are shown in Fig. 4 where Case 3 rearranges the ports to eliminate the  $90^\circ$  turns used in all previous cases. This reveals the two distinct source types just discussed. The radiation efficiency is increased over the one-loop example because there are two half-circles radiating but this is mediated by several competing effects. First, the one-loop case has essentially 3 radiators but with poor spatial overlap (Fig. 3) whereas Case 2 has 4 consisting of two pairs, either of which can overlap exactly while Case 3 has only 2 radiators but these can overlap perfectly at certain frequencies. While there is both constructive and destructive interference occurring, it is clear that Cases 2 and 3 show power doubling between one another at the intermediate frequencies whereas Cases 1 and 3 show a corresponding quadrupling there. While one sees nearly perfect doubling of the power at the lowest two, strong resonances, this gets successively worse with increasing frequency as the characteristic size of the radiator comes into match with the radiated wavelength. Case 1 then begins to compete as the  $90^\circ$  turns begin to dominate.

#### Case 2: 2-Loop, 1-Period, $N=1$ with Different $d$

Figure 2 again shows the simulated structure. The goal here is to achieve a constructive radiation of the two-half circles, using  $d$  as a tuning element to obtain higher radiated power or radiation efficiency as well as directivity. In order to do this, a transmission line of distance  $d$  or some functional equivalent such as multi-port feeds is inserted between the two half-circles. By changing the distance  $d$ , the phase difference of the EM-waves propagating along the two half circles is controlled. It is important to mention that the radiated power will be a

function of only the frequency  $f$  and the distance  $d$  when keeping all the other parameters, e.g. the shape, fixed. FDTD simulation results are shown in Fig. 5, where we observe that the cases for  $d=0.5R$  and  $\pi R$  correspond most closely to Case 2 of Fig. 4, except that the quadratic variation with frequency is more obvious in Fig. 5. Although the  $d=\pi R$  resonance near 16 THz has high efficiency and narrow bandwidth, the peak-to-valley ratio, efficiency, and width of the  $d=2R$  resonance at 18 THz is more remarkable. In this case, the circles are the tuning elements for the  $90^\circ$  turns spaced at  $2R$  i.e. a crenellated structure requiring multi-port feeds appears preferred.

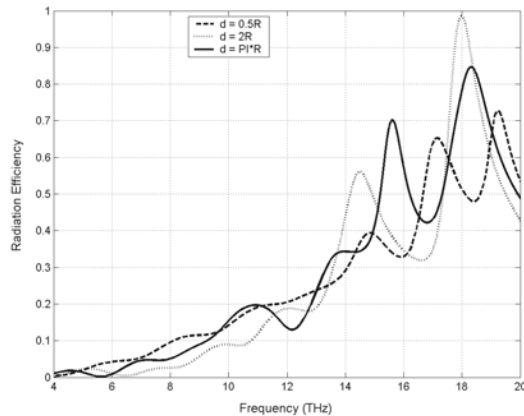


Figure 5: Radiation efficiencies for different  $d$  values.

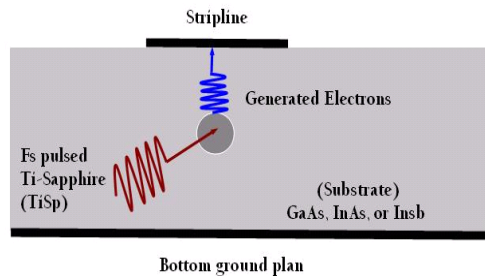


Figure 6: Pulse generation via TiSp on direct band-gaps.

## Monte Carlo Simulations

All of the forgoing EM-analysis was carried out based on predefined, ideal Gaussian pulses. However, in practical cases, generation of such pulses would involve optical excitations, e.g. using Ti-Sapphire lasers. In such cases, the generated electrons due to laser excitation will propagate a predefined distance before reaching a metallic contact (Fig. 6). This implies Monte Carlo simulations to study the effect of distance and conditions on the generated pulse (spatial and temporal shape).

The principle of the Monte Carlo method is to simulate the production and transport of an ensemble of single particle carrier through the source material to the microstrip line. This is done by selecting the duration of the carrier free flights and scattering events stochastically. The simulation is made by generating a sequence of random numbers defining the drift-time and scattering processes. A Monte Carlo code was developed that includes production, followed by impurity scattering, polar and non-polar optical scattering, as well as phonon scattering. Figure 7 shows one step of the problem for one

material - the velocity-electric field relation for bulk GaAs for different temperatures. The mobility (slope in Fig. 7) increases with decreasing temperature because of phonon scattering. The resulting temporal profile depends on the external conditions, materials and laser. The negative resistance results from the transition from  $\Gamma$  to L valleys resulting in a sudden increase in effective mass. To improve this, we can increase the band gap by using InAs or InSb that have very low effective masses ( $\Gamma$ ) and much larger  $\Gamma$ -L separations as well as decrease  $N_I$ .

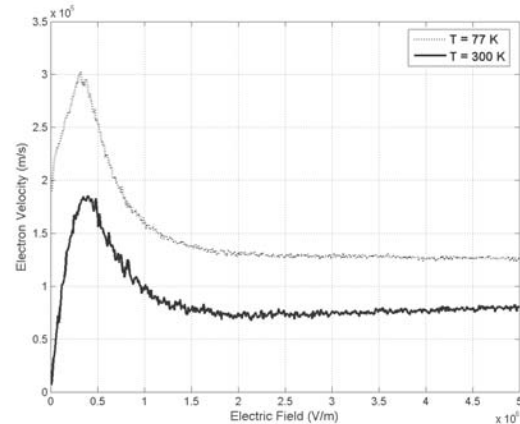


Figure 7: Electron velocity vs E-field calculated for GaAs at 300 & 77° K and impurity concentration  $N_I = 10^{14} \text{ cm}^{-3}$ .

## CONCLUSIONS

We have shown several possible structures that support coherent radiation with a crenellated structure being most interesting. We showed, for one laser driven source scenario, that InAs or InSb is better than GaAs which is better than Si for the laser-driven electron source material. Both Indium compounds are more than four times as efficient in producing electrons than GaAs with InSb 50% better than InAs whereas InAs has a better band gap between  $\Gamma$  and L bands with both far better than GaAs. It remains to be determined which III-V compound is most preferred or practical because this presumably depends on what pulse power is needed i.e. the breakdown voltage.

## REFERENCES

- [1] Y. A. Hussein and J. E. Spencer, "Novel possibilities for coherent radiation sources," *Proc. IEEE MTT-S Int. Sym. Dig.*, 2004, pp.365-368.
- [2] P. H. Siegel, "Terahertz technology," *IEEE Trans. Micro.Theory Tech.*, 50, No. 3, pp. 910-928, 2002.
- [3] P. H. Siegel, "Terahertz technology in biology and medicine," *IEEE Trans. Microwave Theory Tech.*, vol. 52, No. 10, pp. 2438-2447, Oct. 2004.
- [4] The Stanford HEPLs FIREFLY undulator typically produces  $\leq 1$  W of 15-85  $\mu\text{m}$  radiation with a 30 MeV superconducting linac; FELIX produces 20-250  $\mu\text{m}$  at comparable power in the Netherlands.
- [5] A. Taflove, *Computational Electrodynamics:FDTD Method*. Norwood, MA: Artech House, 1995